J. Fluid Mech. (1978), *vol.* 88, *part* 3, *pp.* 499–511
Printed in Great Britain

Acoustic emulsification. Part 1. The instability of the oil–water interface to form the initial droplets

By M. K. LI† AND H. S. FOGLER
Department of Chemical Engineering, University of Michigan, Ann Arbor

(Received 24 June 1977 and in revised form 28 February 1978)

A technique has been developed to study the phenomenon of ultrasonic emulsification in which oil is dispersed as a fine suspension into water at 20 kHz. It was found that the emulsification takes place in two stages. In the first stage, oil droplets of the order of 70 μm are formed from the instability of interfacial waves. In the second stage these large droplets are successively broken into small droplets by cavitation until a stable droplet size is reached. In this paper, the criterion for the instability of the interfacial waves is developed from a linearized stability analysis of the planar oil–water interface exposed to acoustic excitation. The characteristic droplet diameter produced by the instability is related to the induced capillary wavelength at the interface.

The amplitude of the ultrasonic transducer and the theoretical amplitude of vibration necessary for the instability of the interfacial waves were found to be in agreement. In addition, the sizes of the large droplets present in the suspension systems at short irradiation times agree closely with the predicted droplet diameters.

1. Introduction

The phenomenon of ultrasonic emulsification, in which one liquid is dispersed as a fine suspension of another immiscible liquid under the influence of an acoustic field, was discovered half a century ago (Wood & Loomis 1927). The resulting suspensions have qualitatively been known to possess unusual stability characteristics even without the addition of surfactants, and the mean droplet sizes of these suspensions are extremely small and generally lie in the sub-micron region. Because of these two characteristics, the acoustically-formed suspensions may find potential applications in areas where extremely uniform and small particle sizes are essential and where the presence of surfactants is not desirable or is to be kept to a minimum.

Two dominating hypotheses have been promoted in the past to describe the mechanism of ultrasonic liquid–liquid emulsification. The first is the interfacial instability hypothesis. This mechanism depicts the formation of the oil droplets as a result of the unstable growth and eventual eruption of the oil–water interfacial capillary waves induced by the applied acoustic field (Marinesco 1946; Potsis, Yeager & Hovorka 1958; Yeager, Potsis & Hovorka 1961; Fogler 1971). While one may find support for this mechanism from analogous studies of acoustic atomization of liquids (Eisenmenger 1959), one cannot quantitatively correlate the suspension droplet size with the

† Present address: General Electric Corporate Research and Development, Schenectady, New York.

various physical and acoustic parameters of the system. In fact the interfacial instability hypothesis alone cannot account for the sub-micron droplets observed in the acoustically-formed emulsions.

In the second hypothesis the emulsification is believed to be produced as a result of cavitating bubbles near the interface (Sollner & Bondy 1935; Sollner 1938, 1944; Neduzhii 1964, 1965). Despite the qualitative agreement that small oil droplets may be formed by the intense cavitation activity, no one has successfully described the resulting suspension droplet size as a function of the physical parameters of the system and the acoustic parameters associated with the cavitation phenomenon. In addition, and most important, the light microscopes employed in previous work in order to characterize the size of the fluid droplets generally do not yield sufficient resolution and magnification power for precise descriptions of the particle size distributions when the mean sizes are in the sub-micron region. Furthermore, the experimental conditions and procedures have often been either not reported or erroneously chosen (Li 1976). For example, in a study where the cavitation hypothesis was strongly advocated, the effect and significance of acoustic irradiation time was completely ignored (Neduzhii 1964). Based on our work, the irradiation time was found to be a key variable to understanding the acoustic emulsification mechanism. Short acoustic irradiation times of a few seconds produce emulsions with droplet diameters of the order of $70\,\mu$m while one finds the droplets to be of sub-micron size after long irradiation times.

As a result of these problems associated with the acoustic emulsification study, the interpretations of the particle size distributions and the emulsification mechanisms in the past are of dubious value. It is quite evident, therefore, that there is a need not only for developing an improved technique whereby meaningful results may be obtained, but also for devising a mechanistic model to interpret these results.

The present study suggests a two-stage ultrasonic liquid–liquid emulsification mechanism. The first stage involves the initial formation of large droplets of the order of $70\,\mu$m at the oil–water interface by a type of Rayleigh–Taylor instability mechanism. The second stage involves the subsequent breakup of these large droplets into smaller (sub-micron) ones due to the impact of the existing shock waves. These shock waves are continually generated from collapsing cavities produced by the ultrasonic field.

In this paper a theoretical analysis of an oil–water interface is carried out and the criterion for instability of the interfacial waves is derived. Furthermore, a model relating the initial droplet size to the induced interfacial wavelength is used to predict the critical droplet size. A novel technique developed to study the emulsification and solidification of two types of oil–water system is also described in this paper. By solidifying the oil droplets after emulsification a scanning electron microscope can be used to carry out extremely accurate particle size measurements, thereby eliminating the major deficiency of most of the previous work in this area. Finally the theoretical predictions are compared and discussed with the experimental findings at short irradiation times, where the initial droplets from the interfacial instability have not had sufficient time to be broken down by cavitation.

In part 2, the effects of the various parameters (irradiation time, viscosity, interfacial tension, density, etc.) will be presented and discussed in relation to the particle sizes and the distributions of the acoustically-formed suspension systems after long

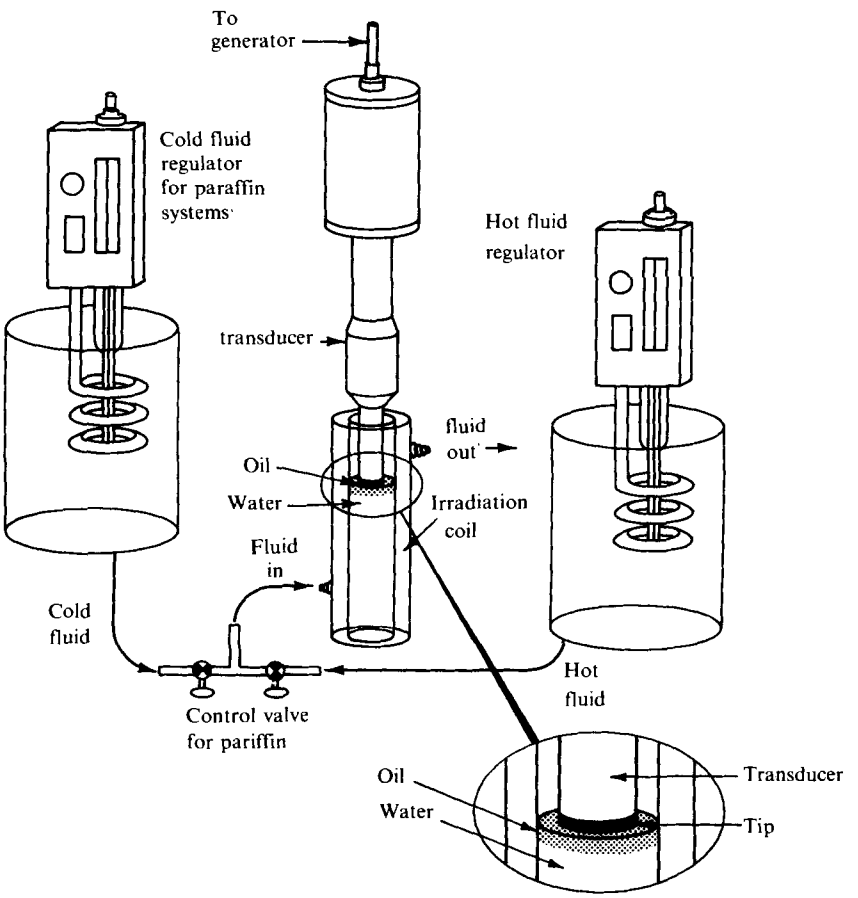

FIGURE 1. Experimental apparatus.

irradiation times. A theoretical model based on the secondary disintegration processes of the large droplets initially formed will be developed for the present liquid–liquid systems. The results obtained from the systems in this study will also be compared with those from gas–liquid systems where the liquid droplets are shattered by the shock impact from the oncoming gas streams.

2. Experimental techniques

In order to follow the changes in the mean particle size and the particle size distribution of suspensions with sub-micron particles, new experimental techniques had to be devised since light microscopes cannot be used with particles of this size. The technique developed was to solidify the oil particles in the emulsion and then to use the high resolution and magnification characteristics of the scanning electron microscope (SEM) for the analyses of sub-micron solid specimens. Since oil–water suspensions generally exist in liquid form, two methods were developed to obtain solid droplets which could then be analysed with the SEM to obtain the mean particle size and particle size distributions of the suspensions. In the first method, an olefin

monomer (monomer styrene) is dispersed into water and followed by a polymerization of the suspended monomer droplets into solid polymer beads. In the second technique, a molten paraffin is dispersed into water and followed by immediate cooling of the suspension below the melting point of the paraffin. This produced a suspension of solid paraffin droplets in water which could be analysed along with the polymer droplets with the SEM. A jacketed irradiation cell which was designed for this purpose is shown in figure 1.

In the polymerization technique, a small quantity (0·03 g/ml styrene) of benzoyl peroxide was dissolved in reagent grade monomer styrene, obtained from Eastman Organic Chemicals, to serve as the initiator for the polymerization of the monomer. Known amounts of this monomer styrene and styrene-saturated water were pippetted into the irradiation cell with the system temperature maintained by circulating temperature-controlled water around the outer jacket. The tip of a step horn transducer was then lowered to near the oil–water interface on the oil side. The transducer was attached to a model W-185 E, Branson Sonic Power Company acoustic generator which was tuned exactly with the horn to produce a frequency of 20 kHz. After the system temperature had attained equilibrium with the circulating water, the sample was irradiated for the time specified. The intensity of the ultrasonic vibration was controlled by choosing and setting the desired intensity level output control on the generator, which has an operating range from 0 to 150 W.

Upon completion of the irradiation, the dispersed monomer styrene–water suspension was transferred to a small vial and then polymerized in a 75 °C oil bath for 8 h. The resulting polymer-in-water suspension was finally sampled, dried and prepared for the scanning electron microscopic analysis.

In the solidification technique, two reagent grade paraffins, octacosane ($C_{28}H_{58}$) and hexatriacontane ($C_{36}H_{74}$), obtained from Eastman Organic Chemicals were chosen for the study. The melting points of the two paraffins are 59–61 °C and 74–76 °C respectively. The paraffin oil was first melted in a test tube, and then transferred by a heated, graduated pippette to the irradiation cell. The emulsification procedure is essentially the same as that for the polymerization method, except that after the irradiation, cooling water was immediately circulated around the outer jacket of the irradiation cell to reduce the system temperature rapidly (about 30 °C for the first 30 s). The resulting paraffin–water suspension is similarly sampled, dried and prepared for the analysis on the SEM. A typical photomicrograph is shown in figure 2 (plate 1).

3. Theory

Owing to the fact that ultrasonic atomization resulted from instability of a fluid–fluid interface (gas–liquid), by analogy it is believed that interfacial instability is involved in at least the first stages of the emulsification process. Further credibility for this hypothesis was demonstrated when it was observed (Fogler 1971) that acoustically induced interfacial wave patterns at a liquid–liquid interface were similar to those observed (Eisenmenger 1959) for gas–liquid interfaces prior to atomization.

In order to describe the response of an oil–water interface to an applied acoustic field, a linear-stability analysis has been employed in § 3.1 to determine the surface wavelength and to establish a criterion for the onset of instability of the interfacial

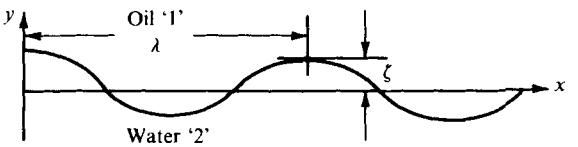

FIGURE 3. Schematic diagram of the liquid–liquid interface.

waves. In acoustic atomization, the droplet diameter was found to be one-third the surface wavelength (Lang 1962). In §3.2, the particle diameter is related to the interfacial wavelength by a rough model in which the crests of the interfacial wave are considered to be cylindrical jets during breakup.

3.1. *Linear-stability analysis of a liquid–liquid interface*

For incompressible liquids subjected to periodic acceleration (figure 3), the vertical component Navier–Stokes equation relative to the accelerating frame may be written as (Yih 1969, pp. 440, 512)

$$\rho\left(\frac{\partial v}{\partial t}+u\frac{\partial v}{\partial x}+v\frac{\partial v}{\partial y}\right)=-\frac{\partial P}{\partial y}+\rho(g_a-g_0\cos\omega_A t)-f_i, \tag{1}$$

where

u_i = velocity component (v = vertical, u = horizontal),
P = pressure at the interface,
g_a = gravitational constant,
$g_0\cos\omega_A t$ = inertial forcing function produced by the oscillation at driving frequency ω_A and acceleration amplitude g_0, and
f_i = a viscous dissipative force.

The viscous force, f_i, will be approximated by assuming that it is proportional to the velocity component u_i,

$$f_i=-4k^2\eta u_i, \tag{2}$$

where k is the interfacial wavenumber and η the viscosity. That f_i could be approximated by (2) was first proposed by Lamb (1945, pp. 399, 624) and later used by Sorokin (1957), Eisenmenger (1959) and by Peskin & Raco (1963). This approximation will account in a rough way for the effects of small dissipative forces without interfering with the irrotational nature of the fluid motion.

Owing to the above approximation, the continuity equation for irrotational flow is written in terms of the velocity potential ϕ,

$$\nabla^2\phi=0, \tag{3}$$

where

$$v=-\frac{\partial\phi}{\partial y}\quad\text{and}\quad u=-\frac{\partial\phi}{\partial x}. \tag{4}$$

After neglecting the second-order inertial terms in (1) and substitution of (2) and (4), the linearized form of the equation of motion in the y direction is

$$-\rho\frac{\partial^2\phi}{\partial y\,\partial t}=-\frac{\partial P}{\partial y}+\rho(g_a-g_0\cos\omega_A t)+4k^2\eta\frac{\partial\phi}{\partial y}.$$

Integrating with respect to y,

$$-\rho\frac{\partial\phi}{\partial t} = -P + P_0 + 4k^2\eta\phi - \rho(g_a + g_0\cos\omega_A t)\,y. \tag{5}$$

Using subscripts 1 and 2 for the oil and water phases respectively, (5) can be written independently for the two liquids as:

$$P_2 = P_0 + 4k^2\eta_2\phi_2 - \rho_2(g_a + g_0\cos\omega_A t)\,y + \rho_2\frac{\partial\phi_2}{\partial t}, \tag{6a}$$

$$P_1 = P_0 + 4k^2\eta_1\phi_1 - \rho_1(g_a + g_0\cos\omega_A t)\,y + \rho_1\frac{\partial\phi_2}{\partial t}. \tag{6b}$$

For the case where the interface of the two fluids is slightly displaced (figure 3), the force balance at the interface is:

$$P_2 - P_1 \approx -\sigma\frac{\partial^2\zeta}{\partial x^2},$$

where σ is the interfacial tension and ζ is the displacement of the interface from its mean position. Setting y equal to ζ and subtracting (6b) from (6a), one obtains:

$$P_2 - P_1 = \left[4k^2(\eta_2\phi_2 - \eta_1\phi_1) - (\rho_2 - \rho_1)(g_a + g_0\cos\omega_A t)\,y + \left(\rho_2\frac{\partial\phi_2}{\partial t} - \rho_1\frac{\partial\phi_1}{\partial t}\right)\right]_{y=\xi}. \tag{7}$$

To assess the time behaviour of (7) for disturbances with a wavenumber k (corresponding to the approximations already made for the viscous forces f_i), we can express ϕ_1 and ϕ_2 as (Lamb 1945, pp. 363 ff.):

$$\phi_1 = A\cos(kx)\,F(t)\exp(-ky), \quad \text{for} \quad y > 0, \tag{8a}$$

$$\phi_2 = -A\cos(kx)\,F(t)\exp(ky), \quad \text{for} \quad y < 0. \tag{8b}$$

These equations satisfy the continuity equation and the condition that the velocity at the interface is continuous [(3) and (4)]. The requirements of vanishing velocity potential at infinity and periodicity in the x direction with a wavenumber of k are also met. Secondly, from the kinematic condition at the interface ($y = \zeta \sim 0$), we have

$$\frac{\partial\zeta}{\partial t} = v\Big|_{y\sim 0} = \frac{\partial\phi_1}{\partial y}\Big|_{y\sim 0} = -\frac{\partial\phi_2}{\partial y}\Big|_{y\sim 0} = Ak\cos(kx)\,F(t). \tag{9}$$

Integration of (9) gives:

$$\zeta = Ak\cos(kx)\int F(t)\,dt. \tag{10}$$

Upon combining (8a, b) and (10) with (7), one finds after simplification that the dynamic condition of the interface can be written as

$$[\sigma k^3 + k(\rho_2 - \rho_1)(g_a + g_0\cos\omega_A t)]\int F(t)\,dt + 4k^2(\eta_1 + \eta_2)\,F(t) + (\rho_1 + \rho_2)\,[dF(t)/dt] = 0. \tag{11}$$

Finally, if we define

$$F(t) = [d\zeta^*(t)/dt], \tag{12}$$

and

$$\zeta^*(t) = M(t)\exp\left[-\frac{2k^2(\eta_1 + \eta_2)\,t}{(\rho_1 + \rho_2)}\right], \tag{13}$$

then (11) may be put into the standard form of the Mathieu equation (McLachlan 1947), viz.

$$[d^2M(\theta)/d\theta^2] + (p - 2q\cos 2\theta)\, M(\theta) = 0, \tag{14}$$

where the parameters p, q and θ are respectively:

$$p = \frac{4k}{\omega_A^2(\rho_1+\rho_2)^2}[\sigma k^2(\rho_1+\rho_2) + (\rho_2^2-\rho_1^2)\, g_a - 4k^3(\eta_1+\eta_2)^2], \tag{15}$$

$$q = -[2k(\rho_2-\rho_1)/(\rho_1+\rho_2)]\,\epsilon, \tag{16}$$

$$\theta = \tfrac{1}{2}\omega_A t,$$

and

$$\epsilon = g_0/\omega_A^2,$$

and ϵ is the amplitude of vibration of the acoustic field.

The solution to the Mathieu equation is:

$$M(\theta) = H(\theta)\exp(\mu\theta), \tag{17}$$

where (Hayashi 1953):

$$H(\theta) = \sin(\theta-\phi_a) + C_3\cos(3\theta-\phi_a) + \ldots + S_3\sin(3\theta-\phi_a) + \ldots, \tag{18}$$

$$C_3 = \tfrac{3}{64}q^2\sin 2\phi_a - \tfrac{1}{512}q^3\sin 4\phi_a + \ldots, \tag{19}$$

$$S_3 = -\tfrac{1}{3}q + \tfrac{1}{64}q\cos 2\phi_a - \tfrac{1}{512}q^3(-\tfrac{14}{3} + 5\cos 4\phi_a) + \ldots, \tag{20}$$

$$\mu = -\tfrac{1}{2}q\sin 2\phi_a + \tfrac{3}{128}q^3\sin 2\phi_a - \tfrac{3}{1024}q^4\sin 4\phi_a + \ldots, \tag{21}$$

and

$$p = 1 - q\cos 2\phi_a - \tfrac{1}{4}q^2(1-\tfrac{1}{2}\cos 4\phi_a) + \tfrac{1}{64}q^3\cos 2\phi_a + \ldots, \tag{22}$$

where the angle ϕ_a determines the phase between the capillary wave oscillation and the acoustic oscillation.

The stability diagram in the p, q space for the solution of a general Mathieu equation is shown in figure 4. The shaded region in figure 4 corresponds to the situation where the interface is unstable. It is seen that even for a small oscillating acceleration amplitude (small g_0), the system can be unstable. In the present analysis, we have confined ourselves in the case of $p \sim 1$ which corresponds to the first eigenvalue of the solution to the Mathieu equation (14) (Yih 1969, p. 515).

It then follows from (10), (12), (13) and (17) that the interfacial displacement, ζ, can be expressed as:

$$\zeta = Ak\cos kx H(\tfrac{1}{2}\omega_A t)\exp\left\{\left[\mu - \frac{4k^2(\eta_1+\eta_2)}{\omega_A(\rho_1+\rho_2)}\right]\frac{\omega_A t}{2}\right\}. \tag{23}$$

The interfacial displacement ζ will have an unbounded growth when the arguments of the exponential term are non-negative, and hence the criterion of the onset of instability is

$$\mu > \mu_c,$$

where

$$\mu_c = \frac{4k^2(\eta_1+\eta_2)}{\omega_A(\rho_2+\rho_1)}. \tag{24}$$

Furthermore, since instability demands the maximum value of μ, it may be easily seen from (21) that this condition will occur at $\phi_a = \frac{1}{4}\pi$. For small values of q, the

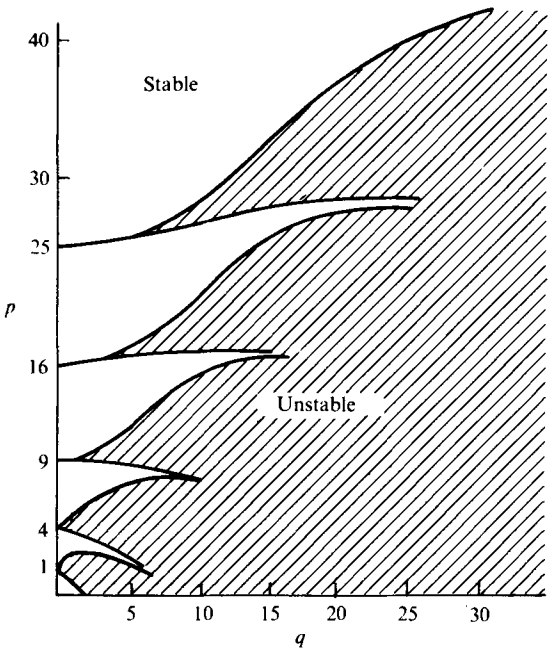

FIGURE 4. The Mathieu diagram.

higher-order terms in q in (16) can be neglected so we can combine (16), (21) and (24) to obtain the instability criterion in terms of the displacement amplitude of vibration:

$$\epsilon > \epsilon_c = \frac{4k(\eta_1+\eta_2)}{\omega_A(\rho_2-\rho_1)}, \quad \phi_a = \tfrac{1}{4}\pi, \tag{25}$$

where ϵ_c is the critical amplitude of acoustic vibration for the onset of instability.

From (25), one observes that the higher the density difference or the smaller the viscosities of the liquids, the more easily the interface can become unstable; whereas for small density difference pairs, the horizontal interface can be made unstable only at higher frequencies or high amplitude of vibration of the acceleration field. Strictly speaking, the linear-stability analysis should apply only at the onset of instability at the interface, however the resulting criterion clearly presents at least the lower limit when the instability can lead to the lamallae of one liquid propagating irreversibly into another liquid.

Once the instability criterion has been fulfilled (i.e. $\epsilon > \epsilon_c$), the resulting particle size is generally believed to be proportional to the capillary wavelength λ, and hence, inversely proportional to the wavenumber k.

In the absence of acoustic and large vertical acceleration fields, the value of the wavenumber k can be calculated by combining (15) and (22) to give:

$$\frac{4k^3}{\omega_A^2(\rho_1+\rho_2)^2}[\sigma(\rho_1+\rho_2)-4k(\eta_1+\eta_2)^2] = 1. \tag{26}$$

However, with the inclusion of the gravitational effect and the applied acoustic field, the wavenumber k, and the other related quantities such as the wavelength, critical amplitude of vibration, etc. must be determined from an iterative procedure

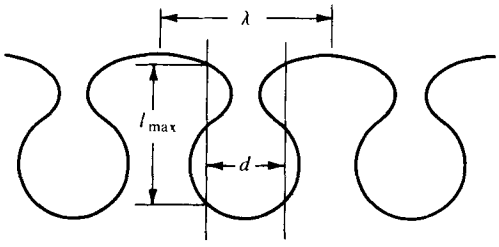

FIGURE 6. Liquid–liquid emulsification model: initial droplet formation.

for a given acceleration g_0. From (15), (16) and (22), however, it may be easily shown that this correction is generally not very significant for low viscosity fluids.

3.2. *Instability of a liquid jet*

In the ultrasonic gas–liquid atomization studies, the mode diameter D is usually correlated with the capillary wavelength as:

$$D = \kappa_1 \lambda, \tag{27}$$

with the value of κ_1 varying from 0·25 to 0·34 (Stamm 1965; Lang 1962). These values actually agree quite well with a model (Doyle *et al.* 1962) which is based on the assumptions that the capillary waves are conical in shape and that a portion of each 'cone' is decapitated to form a droplet when the acceleration forces becomes sufficiently large to result in instability.

However, as observed from the photograph by Pohlman (1969) (figure 5, plate 2) at the instant of the breakup of liquid droplets near the gas–liquid interface, it appears that the droplets are actually breaking away in a manner similar to that of droplets breaking away from a jet issuing from a nozzle or an orifice. This differs qualitatively from the previously suggested cone decapitation model. Consequently, another model based on the criterion for maximum instability of a liquid jet will be considered. In this model, the droplet size, which results from the breakup of such a jet in the initial phase of acoustic emulsification, may be related to the jet wavelength l_{max} (which characterizes the maximum instability) and eventually to the interfacial wavelength λ induced by an acoustic field.

If the jet is depicted as a corrugated cylinder and the velocity of the jet is not appreciable, then

$$\frac{k_{max} d}{2} = \frac{\pi}{l_{max}} d \approx 0{\cdot}707 \tag{28}$$

is the well-known criterion for the maximum instability of a Rayleigh jet (Lamb 1945, p. 471) with a mean jet diameter d. If the drops are formed from a jet that breaks a distance of one wavelength l_{max}, then the droplet volume is equal to the cylinder volume of the broken jet, which has a diameter d and a length of l_{max}, hence:

$$\text{drop volume} = \tfrac{1}{6}\pi D^{*3} = \tfrac{1}{4}\pi d^2 l_{max} = 1{\cdot}111\pi d^3. \tag{29}$$

Experimental confirmation in liquid–liquid systems has been provided by Christiansen & Hixon (1957), who found a value of $D^*/d = 2{\cdot}07$, and by Tyler (1933),

κ_2	0·20	0·33	0·5
Octacosane–water, 72·4 °C	29·0	48·3	72·4
Hexatriacontane–water, 76·5 °C	35·2	58·9	88·3

TABLE 1. Calculated characteristic diameters D^* (μm) for the various systems.

who observed a value of $D^*/d = 1{\cdot}91$. These results agree well with that predicted in (29),

$$D^*/d = 1{\cdot}882,$$

thus the drop will have a diameter nearly twice the mean diameter of the liquid jet at the condition of greatest instability.

In the case of acoustic emulsification, when the criterion necessary for the stability [equation (25)] is exceeded, the growth of the capillary waves is believed to produce a shape of the interface similar to that encountered in the case of ultrasonic atomization (figures 5 and 6). From the above analysis for jet breakup, it will be expected that for $d = \kappa_2 \lambda$ the resulting droplet diameter will be:

$$D^* = 1{\cdot}882d = 1{\cdot}882\kappa_2\lambda, \tag{30}$$

where κ_2 ($0 < \kappa_2 < 1$) is the ratio of the mean diameter d to the interfacial wavelength λ. Therefore, for a given system, the only adjustable parameter in (30) is κ_2.

The value κ_2, estimated from the analysis of Pohlman's photograph (figure 5) for the gas–liquid atomization system is in the range from 0·12 to 0·35 (Li 1976). The derivation of the value of κ_2 from first principles will not be attempted in this work. Instead, on the basis of gas–liquid atomization studies we shall estimate κ_2 to be in the vicinity of 0·5–0·25 for liquid-liquid systems in which the viscosity of the continuous phase is not negligible when compared with the dispersed phase. Table 1 lists the characteristic diameters of the initial droplet sizes expected to be formed for the octacosane–water and the hexatriacontane–water systems at 20 kHz. The wavelength λ, used in calculating the characteristic diameters for these systems, was computed from (15), (16) and (22) for $\epsilon = 60\,\mu$m.

4. Discussion

Critical amplitude of vibration. The linearized stability analysis of an oil–water interface predicts that the interfacial instabilities will lead to the eruption of the oil phase into the water phase when the instability criterion (25) is satisfied. The wavenumber may either be determined in an iterative manner from (15), (16) and (22) for a given amplitude of acceleration, or from (26) when the gravitational acceleration field is neglected.

Table 2 is a summary of the various quantities for the monomer styrene–water, the octacosane–water and the hexatriacontane–water systems at 20 kHz. As shown in the table, the iterative procedure to calculate k using (15), (16) and (22) gives at most 20 % variation from the value obtained from (26).

Measured physical properties	Styrene–water 72·4 °C		$C_{28}H_{58}$–water 72·4 °C		$C_{36}H_{74}$–water 76·5 °C	
ρ_1	0·8603		0·7717		0·7830	
ρ_2	0·9764		0·9764		0·9747	
$\eta_1(P)$	0·00427		0·0423		0·071	
$\eta_2(P)$	0·00394		0·00394		0·00366	
σ (dyne/cm)	28·3		10·4		24·75	
Calculated parameters	*A*	*B*	*A*	*B*	*A*	*B*
q	0	−0·469	0	−1·148	0	−0·890
p	1	0·918	1	0·506	1	0·703
k (cm^{-1})	635·83	617·82	1118·9	816·86	774·56	669·30
λ_k (μm)	98·82	101·70	56·15	76·92	81·12	93·85
ϵ_c (μm)	14·31	13·91	80·46	58·73	96·02	82·97

A From (26).
B Using the iterative procedure from (15), (16) and (22) for $\epsilon = 60\,\mu$m.

TABLE 2. The wavenumber, wavelength and the critical amplitude of vibration for various systems.

Table 2 also shows that the threshold amplitude of vibration (ϵ_c) is in the range 14–80 μm. This agrees closely with the displacement amplitude of vibration of the transducer where the displacement of the transducer tip for the 20 kHz systems at the set intensity is approximately 60 μm. This agreement along with the previously observed acoustically-induced interfacial waves (Fogler 1971) is significant in that it clearly suggests that the interfacial instability is the first stage of liquid–liquid emulsification phenomena at low ultrasonic frequencies (20 kHz).

In addition to the above verification, the third collaborating factor of the present analysis which further supports the interfacial instability hypothesis comes from the measurement of the initial droplet sizes formed from the disruption of the oil–water interface as described below.

Droplet size. As has been pointed out in the introduction, these predicted droplet sizes are of orders of magnitude larger than those observed in a typical suspension system at reasonably *long irradiation* lengths (0·50 min and above; e.g. Sollner & Bondy 1935; Neduzhii 1964). In view of the strong cavitation it should not be too surprising if the large oil droplets were to go through an extremely rapid disintegration process in the present ultrasonic system. In order to observe the droplets with the characteristic dimensions before they are completely disintegrated (if these droplets do exist), therefore, the runs at short irradiation times (0·03–0·10 min) were designed. The 0·03 min irradiation time is the shortest that could be reached owing to inherent lags in the system. After the ultrasonic irradiation and cooling, samples of the paraffin–water suspension were immediately withdrawn from the irradiation cell, and self-dried on the metal stub and then gold-coated. Using the SEM, particles with diameters larger than 10 μm for a given concentration were registered and documented. The results for several runs are listed in table 3 and the numbers (counts) shown were obtained from a direct measurement of photomicrographs from 1 cm^2 SEM stub but are representative of the entire sample.

Run number	Oil–water system	Irradiation time t_I (min)	Number of droplets with diameters greater than 10 μm†	Size of largest particles, μm (number of counts)
1S2–8A	$C_{28}H_{58}$–water	0·03	1420	32·5 (2), 35·0 (1), 57·5 (1)
1S2–8B	$C_{28}H_{58}$–water	0·05	852	30·0 (1), 30·6 (1), 33·3 (1) 35·0 (1), 60·0 (1), 66·7 (1)
1S2–2C	$C_{28}H_{58}$–water	0·10	820	30·0 (1), 31·7 (1), 35·8 (1) 37·5 (1)
2S1–8A	$C_{36}H_{74}$–water	0·03	3606	60·00 (4), 60·8 (4), 61·7 (1) 66·7 (1), 70·0 (2), 71·7 (1) 73·3 (1), 74·2 (2), 75·0 (1) 83·3 (2), 85·0 (1), 86·7 (1) 89·1 (3), 100·0 (1), 103·3 (1) 106·7 (1), 109·1 (1)
2S1–8*B*	$C_{36}H_{74}$–water	0·05	2265	69·2 (1)

† Standardized to account for different suspension concentrations from run to run.

TABLE 3. Results of large particles found in short irradiation time runs.

From experimental data for each of the paraffin–water systems in table 3, one can observe that the range of the *largest* particle size is from 37·5 to 66·7 μm for the octacosane–water system and 69·2 to 109·1 μm for the hexatriacontane–water system. One notes a droplet initially at 109 μm which divides into two equal droplets which divide again to produce 4 droplets 68 μm in diameter. One also observes that the large droplets are rapidly disappearing from the systems with time, and as a result, the largest sizes of the particles also decrease as irradiation time increases. Nevertheless, from the estimated characteristic droplet diameters predicted in table 1 (the largest droplet sizes are 72·4 and 88·3 μm for the $C_{28}H_{58}$–H_2O and $C_{36}H_{74}$–H_2O systems), it is evident that the observed particle sizes do conform quite well to the predicted values from the interfacial instability hypothesis.

Conclusions. A two-stage ultrasonic emulsification mechanism of a liquid–liquid system is proposed. The first stage was of primary concern in this paper. In this stage, the application of an acoustic field produces interfacial waves which become unstable, resulting eventually in the eruption of the oil phase into the water medium in the form of droplets. The criterion for the stability of an oil–water interface was derived from a linearized stability analysis, and a model was then presented, in which the characteristic diameter of the droplet resulting from such an instability was expressed as a function of the induced capillary wavelength at the interface.

The first stage of the mechanism was substantiated from the fact that: (*a*) acoustically induced interfacial waves similar to those for gas–liquid systems have been observed for a liquid–liquid system, (*b*) the amplitude of vibration of the transducer, was found to agree remarkably with the theoretically-predicted threshold amplitude required for the onset of the interfacial instability at the oil–water interface ($\sim$ 14–80 μm), and (*c*) large particles of the order of 40–100 μm were observed at short irradiation time runs for the octacosane–water and the hexatriacontane–water

systems. These results agree again with the theoretical model where droplets are assumed to break off from the oil–water interface in the form of 'capillary-jets', once the instability criterion (the threshold amplitude) is exceeded.

REFERENCES

CHRISTIANSEN, R. M. & HIXON, A. N. 1957 *Ind. Engng Chem.* **49**, 1017.

DOYLE, A. W., MOKLER, B. V., PERRON, R. R. & LITTLE, A. D. 1962 *Am. Petrol. Inst. Publ.* no. 1701, New York.

EISENMENGER, W. 1959 *Acustica* **9**, 327.

FOGLER, H. S. 1971 *Chem. Engng Prog. Symposium Series*, vol. 67, no. 109, p. 1.

HAYASHI, C. 1953 *Forced Oscillation in Non-linear Systems*. Tokyo: Nippon Printing and Publishing Co.

LAMB, H. 1945 *Hydrodynamics*. Dover.

LANG, R. J. 1962 *J. Acoust. Soc. Am.* **34**, 6.

LI, M. K. 1976 Ph.D. thesis, The University of Michigan.

MCLACHLAN, N. W. 1947 *Theory and Application of Mathieu Functions*. Oxford University Press.

MARINESCO, N. 1946 *Chem. Ind.* **55** (2), 87.

NEDUZHII, S. A. 1964 *Sov. Phys. Acoust.* **9**, 195.

NEDUZHII, S. A. 1965 *Sov. Phys. Acoust.* **10**, 390.

PESKIN, R. L. & RACO, R. J. 1963 *J. Acoust. Soc. Am.* **35**, 1378.

POHLMAN, R. 1969 *Fraunhofer-Ges. (Examples of Applied Research)*, p. 136.

POTSIS, A., YEAGER, E. & HOVORKA, F. 1958 *J. Acoust. Soc. Am.* **30**, 678.

SOLLNER, K. 1938 *J. Phys. Chem.* **42**, 1071.

SOLLNER, K. 1944 *Colloid Chemistry* (ed. J. Alexander), vol. 5. Reinhold.

SOLLNER, K. & BONDY, C. 1935 *Trans. Farad. Soc.* **31**, 835.

SOROKIN, V. I. 1957 *Sov. Phys. Acoust.* **3**, 281.

STAMM, K. 1965 *Tech. Mitt.* **58** (3), 109.

TYLER, E. 1933 *Phil. Mag.* **16**, 504.

WOOD, R. W. & LOOMIS, A. L. 1927 *Phil. Mag.* **4**, 417.

YEAGER, E., POTSIS, A. & HOVORKA, F. 1961 *Proc. 3rd Int. Cong. on Acoustics*, vol. 2, p. 1276, Amsterdam-London-N.Y.

YIH, C. S. 1969 *Fluid Mechanics*. McGraw-Hill.

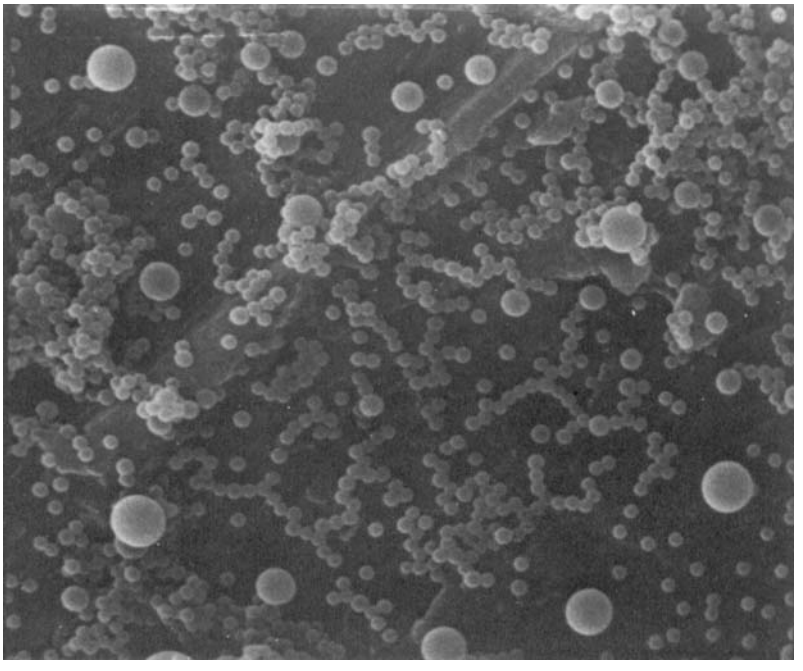

FIGURE 2. Typical microphotograph of cavitation-formed emulsions of styrene in water. Irradiation time = 2·00 min. Mean particle size = 0·16 μm.

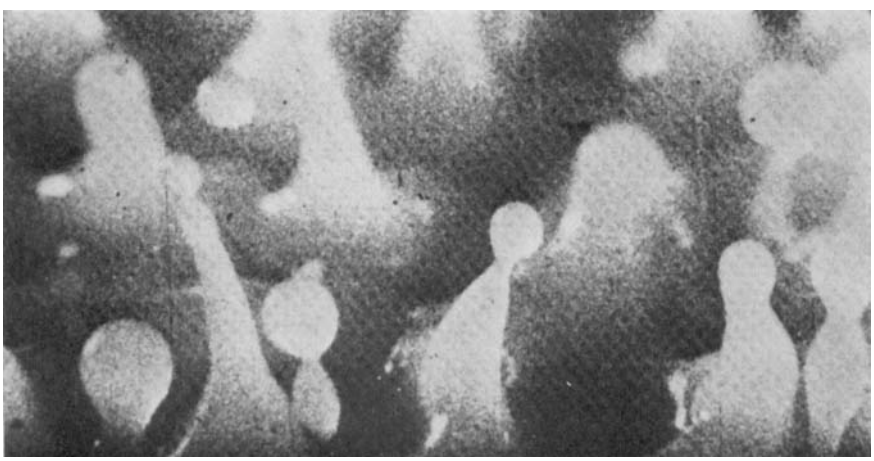

FIGURE 5. Onset of the gas–liquid atomization process (Pohlman 1969).